

AIR algebraic multigrid for a space-time hybridizable discontinuous Galerkin discretization of advection(-diffusion)*

A. A. Sivas[†]B. S. Southworth[‡]S. Rhebergen[§]

February 1, 2022

Abstract

This paper investigates the efficiency, robustness, and scalability of approximate ideal restriction (AIR) algebraic multigrid as a preconditioner in the *all-at-once* solution of a space-time hybridizable discontinuous Galerkin (HDG) discretization of advection-dominated flows. The motivation for this study is that the time-dependent advection-diffusion equation can be seen as a “steady” advection-diffusion problem in $(d + 1)$ -dimensions and AIR has been shown to be a robust solver for steady advection-dominated problems. Numerical examples demonstrate the effectiveness of AIR as a preconditioner for advection-diffusion problems on fixed and time-dependent domains, using both slab-by-slab and all-at-once space-time discretizations, and in the context of uniform and space-time adaptive mesh refinement. A closer look at the geometric coarsening structure that arises in AIR also explains why AIR can provide robust, scalable space-time convergence on advective and hyperbolic problems, while most multilevel parallel-in-time schemes struggle with such problems.

1 Introduction

In this paper, we are interested in the fast parallel solution of the time-dependent advection(-diffusion) problem on a time-dependent domain $\Omega(t)$,

$$\partial_t u + a \cdot \nabla u - \nu \nabla^2 u = f \quad \text{in } \Omega(t), \quad t^0 < t < t^N, \quad (1)$$

where a is the advective velocity, f is a source term, and $\nu \geq 0$ is the diffusion constant. We are particularly interested in the advection-dominated regime where $0 \leq \nu \ll 1$.

To discretize eq. (1), we consider the space-time framework in which the problem is recast into a space-time domain as follows. Let $x = (x_1, \dots, x_d)$ be the spatial variables in spatial dimension d . A point at time $t = x_0$ with position x then has Cartesian coordinates $\hat{x} = (x_0, x)$ in space-time. Defining the space-time domain $\mathcal{E} := \{\hat{x} : x \in \Omega(x_0), t^0 < x_0 < t^N\}$, the space-time advective velocity $\hat{a} := (1, a)$ and the space-time gradient $\hat{\nabla} := (\partial_t, \nabla)$, the space-time formulation of eq. (1) is given by

$$\hat{a} \cdot \hat{\nabla} u - \nu \nabla^2 u = f \quad \text{in } \mathcal{E}. \quad (2)$$

*SR gratefully acknowledges support from the Natural Sciences and Engineering Research Council of Canada through the Discovery Grant program (RGPIN-05606-2015). BSS was supported by Lawrence Livermore National Laboratory under contracts B639443 and B634212, and as a Nicholas C. Metropolis Fellow under the Laboratory Directed Research and Development program of Los Alamos National Laboratory.

[†]Department of Applied Mathematics, University of Waterloo, Canada (aasivas@uwaterloo.ca), <http://orcid.org/0000-0002-5263-1889>

[‡]Los Alamos National Laboratory, Los Alamos NM, U.S.A. (southworth@lanl.gov), <http://orcid.org/0000-0002-0283-4928>

[§]Department of Applied Mathematics, University of Waterloo, Canada (srheberg@uwaterloo.ca), <http://orcid.org/0000-0001-6036-0356>

There are multiple reasons to consider space-time finite element methods over traditional discretizations. First, space-time methods provide a natural framework for the discretization of partial differential equations on time-dependent domains [24, 33, 48, 49, 53]. This is because the domain and mesh movement are automatically accounted for by the space-time finite element spaces, which are defined on a triangulation of the space-time domain \mathcal{E} . Furthermore, since there is no distinction between spatial and temporal variables, it is relatively straightforward to allow local time stepping and adaptive space-time mesh refinement (see, for example [52]). This is particularly interesting from an efficiency perspective for problems that require locally small time steps and fine mesh resolution to achieve high levels of accuracy in only some parts of the domain. These properties are non-trivial within the context of traditional time-integration techniques. Finally, space-time finite elements allow for greater parallelization by solving for the entire space-time solution simultaneously, rather than in a sequential time-stepping process. This ends up being particularly relevant for hyperbolic PDEs, as will be discussed later.

Space-time discontinuous Galerkin (DG) finite element methods are well suited for solving eq. (2) in the advection-dominated limit (see [38, 45, 46, 47, 50, 51, 54] and references therein). This is because space-time DG methods incorporate upwinding in their numerical fluxes, are locally conservative, and automatically satisfy the geometric conservation law (GCL) [27], which requires that the uniform flow remains uniform under grid motion. We point out that alternative discretizations (such as arbitrary Lagrangian–Eulerian methods) may require additional constraints to satisfy the GCL [35]. One downside of space-time DG methods is the large number of globally coupled degrees-of-freedom (DOFs) that arise when applying DG finite elements in $(d + 1)$ -dimensional space. However, the space-time hybridizable discontinuous Galerkin (HDG) method [36, 37], introduced as a space-time extension of the HDG method [8], can attenuate this problem. The space-time HDG method, like the HDG method, introduces approximate traces of the solution on the element faces. The DOFs on the interior of an element are then eliminated from the system, resulting in a (significantly smaller) global system of algebraic equations only for the approximate traces. However, it should be noted that a reduction in the number of globally coupled DOFs does not necessarily imply a more efficient time to solution – the linear system still needs to be solved.

In practice, a *slab-by-slab* approach is almost exclusively used to obtain the solution of space-time discretizations, which is analogous to traditional time-integration techniques: the space-time domain is partitioned into space-time slabs and local systems are solved sequentially one time step after the other (e.g. [25, 33, 51]). Although commonly used, such an approach is limited to spatial parallelism, which eventually plateaus in the sense that using more processors does not speed up the time to the solution (see, e.g., [14]). With an increasing number of processors available for use and stagnating core clock speeds, there has been significant research on parallel-in-time (PinT) methods in recent years.

Some of the most effective PinT methods are multigrid-in-time methods, where a parallel multilevel method is applied over the time domain, which is then coupled with traditional spatial solves to perform time steps of varying sizes (in particular, see Parareal [28] and multigrid-reduction-in-time [14]). Such methods are effective on parabolic-type problems, but tend to not be robust or just not convergent on advection-dominated and hyperbolic problems without special treatment (for example, see [41, 16, 12, 9, 11]). The simplest explanation for the difficulties such methods have with hyperbolic problems is the separation of space and time. By treating space and time separately, the multilevel coarsening cannot respect the underlying characteristics that propagate in space-time.

A more general approach is to consider space-time multigrid, that is, multigrid methods applied to the full space-time domain. To our knowledge, such an approach has only been applied to parabolic problems, primarily the heat equation [55, 21, 17]. However, even there, space-time multigrid has demonstrated superior performance over PinT methods that use multigrid in space and time separately [15]. Recently, auxiliary-space preconditioning techniques have also been proposed for space-time finite-element discretizations [18], which has the potential to provide more general space-time solvers. Continuing with the above discussion, the *all-at-once* approach to space-time finite elements constructs and solves a single global linear system for the solution in the whole space-time domain. From a solver’s perspective, we claim that the all-at-once approach is particularly well suited for advective and hyperbolic problems.

The main contribution of this paper is demonstrating the suitability of the nonsymmetric algebraic

multigrid (AMG) method based on Approximate Ideal Restriction (AIR) [30, 32] for the solution of slab-by-slab and, in particular, all-at-once space-time HDG discretizations of the advection-diffusion problem in advection-dominated regimes. Advection-dominated problems are typically difficult to solve due to the non-symmetric nature of the problem. Nevertheless, significant developments in multigrid methods for non-symmetric problems have been made in recent years [34, 57, 6, 42, 31]. In particular, AIR has shown to be a robust solver for steady advection-dominated problems. This motivates us to study AIR for a space-time HDG discretization of the advection-diffusion problem, since eq. (2) can be seen as a “steady” advection-diffusion problem in $(d + 1)$ -dimensions.

The remainder of this paper is organised as follows. In section 2, we present the space-time HDG discretization of the advection-diffusion equation, and AIR is presented in section 3. A discussion on why AIR can be effective as a space-time solver of advection-dominated problems, while most PinT methods struggle, is provided in section 3.1. Numerical results in section 4 indeed demonstrate that AIR is a robust and scalable solver for space-time HDG discretizations of the advection-diffusion equation. Scalable preconditioning is demonstrated with space-time adaptive mesh refinement (AMR) and on time-dependent domains, and speedups over sequential time stepping are obtained on very small processor counts. We draw conclusions in section 5.

2 The space-time HDG method for the advection-diffusion equation

2.1 The advection-diffusion problem on time-dependent domains

Let $\Omega_h(t) \subset \mathbb{R}^d$, an approximation to the domain $\Omega(t)$ in eq. (1), be a polygonal ($d = 2$) or polyhedral ($d = 3$) domain whose evolution depends continuously on time $t \in [t^0, t^N]$. We will present numerical results only for the case $d = 2$, but remark that the space-time HDG discretization and solution procedure also hold for $d = 3$. We partition the boundary of $\Omega_h(t)$, $\partial\Omega_h(t)$, into two sets $\Gamma_D(t)$ (the Dirichlet boundary) and $\Gamma_N(t)$ (the Neumann boundary) such that $\partial\Omega_h(t) = \Gamma_D(t) \cup \Gamma_N(t)$ and $\Gamma_D(t) \cap \Gamma_N(t) = \emptyset$.

As discussed in section 1, a point in space-time at time $t = x_0$ with position x has Cartesian coordinates $\hat{x} = (x_0, x)$. Throughout this paper, we will use t and x_0 interchangeably. We introduce the $(d + 1)$ -dimensional computational space-time domain $\mathcal{E}_h := \{\hat{x} : x \in \Omega_h(x_0), t^0 < x_0 < t^N\} \subset \mathbb{R}^{d+1}$. The boundary of \mathcal{E}_h is comprised of the hyper-surfaces $\Omega_h(t^0) := \{\hat{x} \in \partial\mathcal{E}_h : x_0 = t^0\}$, $\Omega_h(t^N) := \{\hat{x} \in \partial\mathcal{E}_h : x_0 = t^N\}$, and $\mathcal{Q}_{\mathcal{E}_h} := \{\hat{x} \in \partial\mathcal{E}_h : t^0 < x_0 < t^N\}$. We also introduce the partitioning $\partial\mathcal{E}_h = \partial\mathcal{E}_D \cup \partial\mathcal{E}_N$ where $\partial\mathcal{E}_D := \{\hat{x} : x \in \Gamma_D(x_0), t^0 < x_0 < t^N\}$ and $\partial\mathcal{E}_N := \{\hat{x} : x \in \Gamma_N(x_0) \cup \Omega(t^0), t^0 < x_0 \leq t^N\}$. The outward unit space-time normal vector to $\partial\mathcal{E}_h$ is denoted by $\hat{n} = (n_t, n)$, where $n_t \in \mathbb{R}$ is the temporal part of the space-time vector and $n \in \mathbb{R}^d$ the spatial part.

Given the viscosity $\nu \geq 0$, forcing term $f : \mathcal{E}_h \rightarrow \mathbb{R}$, and advective velocity $a : \mathcal{E}_h \rightarrow \mathbb{R}^d$, the advection-diffusion equation for the scalar $u : \mathcal{E}_h \rightarrow \mathbb{R}$ is given by

$$\partial_t u + a \cdot \nabla u - \nu \nabla^2 u = f \quad \text{in } \mathcal{E}_h, \quad (3a)$$

$$-\zeta u(n_t + a \cdot n) + \nu \nabla u \cdot n = g_N \quad \text{on } \partial\mathcal{E}_N, \quad (3b)$$

$$u = g_D \quad \text{on } \partial\mathcal{E}_D, \quad (3c)$$

where $g_N : \mathcal{Q}_N \rightarrow \mathbb{R}$ is a suitably smooth function and ζ is an indicator function for the inflow boundary of \mathcal{E} , i.e., where $(n_t + a \cdot n) < 0$. Note that the initial condition $u(0, x) = g_N(0, x)$ is imposed by eq. (3b). Using the definition of the space-time advective velocity and the space-time gradient introduced in section 1, the space-time formulation of eq. (3) is given by

$$\hat{a} \cdot \hat{\nabla} u - \nu \nabla^2 u = f \quad \text{in } \mathcal{E}_h, \quad (4a)$$

$$-\zeta u \hat{a}_n + \nu \nabla u \cdot n = g_N \quad \text{on } \partial\mathcal{E}_N, \quad (4b)$$

$$u = g_D \quad \text{on } \partial\mathcal{E}_D, \quad (4c)$$

where $\hat{a}_n = \hat{n} \cdot \hat{a} = n_t + a \cdot n$. We see that the time-dependent advection-diffusion problem eq. (3) is a steady state problem in $(d + 1)$ -dimensional space-time.

2.2 Space-time meshes

The two approaches to meshing a space-time domain \mathcal{E}_h are the slab-by-slab approach and the all-at-once approach. In the *slab-by-slab* approach, the time interval $[t^0, t^N]$ is partitioned into time levels $t^0 < t^1 < \dots < t^N$. The n -th time interval is defined as $I^n = (t^n, t^{n+1})$ and its length is the “time-step”, denoted by $\Delta t^n = t^{n+1} - t^n$. The space-time domain \mathcal{E}_h is then divided into space-time slabs $\mathcal{E}_h^n = \mathcal{E}_h \cap (I^n \times \mathbb{R}^d)$. Note that each space-time slab \mathcal{E}_h^n is bounded by $\Omega_h(t^n)$, $\Omega_h(t^{n+1})$, and $\mathcal{Q}_{\mathcal{E}_h^n} = \partial\mathcal{E}_h^n \setminus (\Omega_h(t^n) \cup \Omega_h(t^{n+1}))$. A space-time triangulation \mathcal{T}_h^n is then introduced for each space-time slab \mathcal{E}_h^n using standard spatial meshing techniques. In this paper, we use space-time simplices (see, e.g. [22, 23, 54]) as opposed to space-time hexahedra (see e.g. [3, 51, 52]).

In the *all-at-once* approach, a space-time triangulation $\mathcal{T}_h := \cup_j \mathcal{K}_j$ of the full space-time domain \mathcal{E}_h is introduced. This triangulation consists of non-overlapping space-time simplices $\mathcal{K} \subset \mathbb{R}^{d+1}$. There are no clear time levels except for the time level at $x_0 = t^0$ and $x_0 = t^N$ and the space-time mesh may be fully unstructured. In particular, this naturally allows for arbitrary adaptive mesh refinement (AMR) in space and time. Note, we do not consider hanging nodes in this paper although hanging nodes in space and time are possible within the space-time framework.

In fig. 1 we plot space-time elements in a slab-by-slab approach and in an all-at-once approach in $(1+1)$ -dimensional space-time.

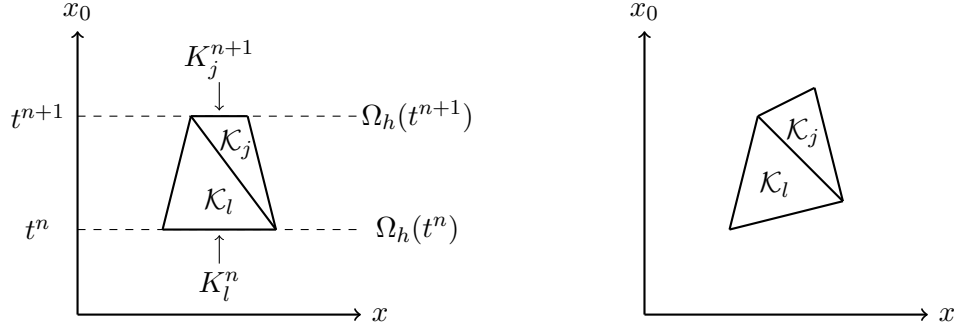


Figure 1: Examples of two neighboring elements in $(1+1)$ -dimensional space-time. Left: An example of space-time elements in a slab-by-slab approach. The space-time mesh is layered by space-time slabs. Here the elements lie in space-time slab \mathcal{E}_h^n . Right: An example of space-time elements in an all-at-once approach. There are no clear time levels for $t^0 < x_0 < t^N$.

2.3 The space-time HDG method

Consider a space-time element $\mathcal{K} \in \mathcal{T}_h$ in an all-at-once or slab-by-slab mesh. On the boundary of a space-time element $\partial\mathcal{K}$ we will denote the outward unit space-time normal vector by $\hat{n}^\mathcal{K} = (n_t^\mathcal{K}, n^\mathcal{K})$. Two adjacent space-time elements \mathcal{K}^+ and \mathcal{K}^- share an interior space-time facet $\mathcal{S} := \partial\mathcal{K}^+ \cap \partial\mathcal{K}^-$. A facet of $\partial\mathcal{K}$ that lies on the space-time boundary $\partial\mathcal{E}_h$ is called a boundary facet. The set of all facets is denoted by \mathcal{F} and the union of all facets by Γ_0 . For ease of notation, we will drop the subscripts and superscripts when referring to space-time elements, their boundaries, and outward unit normal vectors in the remainder of this article.

We require the following finite element spaces:

$$\begin{aligned} V_h &:= \{v_h \in L^2(\mathcal{E}_h) : v_h|_{\mathcal{K}} \in P_p(\mathcal{K}), \forall \mathcal{K} \in \mathcal{T}_h\}, \\ M_h &:= \{\mu_h \in L^2(\mathcal{F}) : \mu_h|_{\mathcal{S}} \in P_p(\mathcal{S}), \forall \mathcal{S} \in \mathcal{F}, \mu_h = 0 \text{ on } \partial\mathcal{E}_D\}, \end{aligned}$$

where $P_p(D)$ is the set of polynomials of degree p on a domain D . We furthermore introduce $V_h^\star := V_h \times M_h$. The space-time HDG method for eq. (4) is given by [26]: find $(u_h, \lambda_h) \in V_h^\star$ such that

$$\mathcal{B}_h((u_h, \lambda_h), (v_h, \mu_h)) = \sum_{\mathcal{K} \in \mathcal{T}_h} \int_{\mathcal{K}} f v_h d\hat{x} + \int_{\partial\mathcal{E}_N} g \mu_h ds \quad \forall (v_h, \mu_h) \in V_h^\star, \quad (5)$$

where the bilinear form is defined as

$$\begin{aligned} \mathcal{B}_h((u, \lambda), (v, \mu)) &:= \sum_{\mathcal{K} \in \mathcal{T}_h} \int_{\mathcal{K}} (-u \hat{a} \cdot \hat{\nabla} v + \nu \nabla u \cdot \nabla v) d\hat{x} + \int_{\partial \mathcal{E}_N} \frac{1}{2} (\hat{a}_n + |\hat{a}_n|) \lambda \mu ds \\ &\quad + \sum_{\mathcal{K} \in \mathcal{T}_h} \int_{\partial \mathcal{K}} \sigma(u, \lambda, \hat{n})(v - \mu) ds - \sum_{\mathcal{K} \in \mathcal{T}_h} \int_{\partial \mathcal{K}} \nu(u - \lambda) \nabla v \cdot n ds. \end{aligned} \quad (6)$$

Here $\sigma(u, \lambda, \hat{n}) := \sigma_a(u, \lambda, \hat{n}) + \sigma_d(u, \lambda, n)$ is the “numerical flux” on the cell facets. The advective part of the numerical flux is an upwind flux in both space and time, given by

$$\sigma_a(u, \lambda, \hat{n}) := \frac{1}{2} (\hat{a}_n(u + \lambda) + |\hat{a}_n|(u - \lambda)).$$

The diffusive part of the numerical flux is similar to that of an interior penalty method and is given by

$$\sigma_d(u, \lambda, n) := -\nu \nabla u \cdot n + \frac{\nu \alpha}{h_{\mathcal{K}}}(u - \lambda), \quad (7)$$

with $h_{\mathcal{K}}$ the length measure of the element \mathcal{K} , and $\alpha > 0$ a penalty parameter. It is shown in [26] that α needs to be sufficiently large to ensure stability of the space-time HDG method.

2.4 Sequential time-stepping using the slab-by-slab discretization

The space-time HDG method eq. (5) is the same for both the slab-by-slab and all-at-once space-time approaches. However, for the slab-by-slab approach we may write eq. (5) in a form similar to traditional time-integration techniques. For this we require the following finite element spaces:

$$\begin{aligned} V_h^n &:= \{v_h \in L^2(\mathcal{E}_h^n) : v_h|_{\mathcal{K}} \in P_p(\mathcal{K}), \forall \mathcal{K} \in \mathcal{T}_h^n\}, \\ M_h^n &:= \{\mu_h \in L^2(\mathcal{F}^n) : \mu_h|_{\mathcal{S}} \in P_p(\mathcal{S}), \forall \mathcal{S} \in \mathcal{F}^n, \mu_h = 0 \text{ on } \partial \mathcal{E}_D^n\}, \end{aligned}$$

where \mathcal{F}^n is the set of all facets in the slab \mathcal{E}_h^n . We furthermore define $V_h^{n,*} := V_h^n \times M_h^n$. For the slab-by-slab approach, we may write the space-time HDG method for eq. (3) as: for each space-time slab \mathcal{E}_h^n , $n = 0, 1, \dots, N-1$, find $(u_h, \lambda_h) \in V_h^{n,*}$ such that

$$\mathcal{B}_h^n((u_h, \lambda_h), (v_h, \mu_h)) = \sum_{\mathcal{K} \in \mathcal{T}_h^n} \int_{\mathcal{K}} f v_h d\hat{x} + \int_{\partial \mathcal{E}_N^n} g \mu_h ds, \quad (8)$$

for all $(v_h, \mu_h) \in V_h^{n,*}$, where $\mathcal{B}_h^n(\cdot, \cdot)$ is defined as eq. (6) but with \mathcal{T}_h and $\partial \mathcal{E}_N$ replaced by, respectively, \mathcal{T}_h^n and $\partial \mathcal{E}_N^n$. The slab-by-slab approach is similar to traditional time-integration techniques in that the local systems are solved one space-time slab after another. The linear systems arising from space-time finite elements resemble those that arise from fully implicit Runge–Kutta methods (e.g., see [29, 43]).

Well-posedness and convergence of the slab-by-slab space-time HDG method eq. (8) was proven in [26]. Furthermore, motivated by the fact that the spatial mesh size h_K and the time-step Δt may be different, an a priori error analysis was presented in [26], resulting in optimal error bounds that are anisotropic in h_K (a measure of the mesh size in spatial direction) and Δt . It is shown, however, that Δt and h_K need to be refined simultaneously to obtain these optimal error bounds, and that refining only in time or only in space may lead to divergence of the error. To this end, all-at-once solvers seem like the natural solution for efficient parallel simulations, where simultaneous local adaptivity in space and time is easily handled.

2.5 The discretization

Let $U \in \mathbb{R}^r$ be the vector of expansion coefficients of u_h with respect to the basis for V_h and let $\Lambda \in \mathbb{R}^q$ be the vector of expansion coefficients of λ_h with respect to the basis for M_h . The space-time HDG method

eq. (5) can then be expressed as the all-at-once system of linear equations

$$\begin{bmatrix} A & B \\ C & D \end{bmatrix} \begin{bmatrix} U \\ \Lambda \end{bmatrix} = \begin{bmatrix} F \\ G \end{bmatrix}, \quad (9)$$

where A , B , C , and D are matrices obtained from the discretization of $\mathcal{B}_h((\cdot, 0), (\cdot, 0))$, $\mathcal{B}_h((0, \cdot), (\cdot, 0))$, $\mathcal{B}_h((\cdot, 0), (0, \cdot))$, and $\mathcal{B}_h((0, \cdot), (0, \cdot))$, respectively.

For the slab-by-slab approach, the linear system eq. (9) can be decoupled into smaller linear systems that are solved in each time slab \mathcal{E}_h^n . In this case, $U \in \mathbb{R}^r$ is the vector of expansion coefficients of u_h with respect to the basis for V_h^n and $\Lambda \in \mathbb{R}^q$ is the vector of expansion coefficients of λ_h with respect to the basis for M_h^n . Furthermore, A , B , C , and D are then the matrices obtained from the discretization of $\mathcal{B}_h^n((\cdot, 0), (\cdot, 0))$, $\mathcal{B}_h^n((0, \cdot), (\cdot, 0))$, $\mathcal{B}_h^n((\cdot, 0), (0, \cdot))$, and $\mathcal{B}_h^n((0, \cdot), (0, \cdot))$, respectively.

The space-time HDG discretization is such that A is a block-diagonal matrix. Using $U = A^{-1}(F - B\Lambda)$ we eliminate U from eq. (9) resulting in the following reduced system for Λ :

$$S\Lambda = H, \quad (10)$$

where $S = D - CA^{-1}B$ is the Schur complement of the block matrix in eq. (9), and $H = G - CA^{-1}F$. Having eliminated the element degrees-of-freedom via static condensation, the linear system eq. (10) is significantly smaller than eq. (9). However, for the space-time HDG method to be efficient, we still require a fast solver for the reduced non-symmetric problem eq. (10), which is discussed in the following section.

3 Approximate ideal restriction (AIR) AMG

AMG is traditionally designed for elliptic problems in space or sequential time stepping of parabolic problems, where the resulting linear systems are (nearly) symmetric positive definite or M-matrices. However, a number of papers in recent years have considered extensions of AMG to the nonsymmetric setting, e.g., [34, 57, 6, 42, 31]. In particular, a new AMG method based on a local approximate ideal restriction (ℓ AIR; moving forward we simply refer to it as AIR) was developed in [30, 32] specifically for advection-dominated problems and upwinded discretizations. Noting that eq. (4) is a “steady” advection-dominated problem in $(d+1)$ -dimensional space-time, and that AIR is a robust solver for advection dominated problems, motivates the use of AIR as a preconditioner for the space-time linear system eq. (10).

As a brief review, recall that multigrid methods solve $A\mathbf{x} = \mathbf{b}$ by applying a coarse-grid correction based on interpolation and restriction operators, $\mathbf{x}^{(i+1)} = \mathbf{x}^{(i)} + P(RAP)^{-1}R\mathbf{r}^{(i)}$, for matrix A , interpolation P , restriction R , and residual $\mathbf{r}^{(i)} = \mathbf{b} - A\mathbf{x}^{(i)}$. Classical AMG is based on a partitioning of DOFs into fine (F-) and coarse (C-) points, where A can then be expressed in block form as

$$A = \begin{bmatrix} A_{ff} & A_{fc} \\ A_{cf} & A_{cc} \end{bmatrix}.$$

AIR is a reduction method based on the principle that if we use the so-called ideal restriction operator, $R_{\text{ideal}} = [-A_{cf}A_{ff}^{-1} \quad I]$ with any interpolation (in MATLAB notation) $P = [W; I]$, coarse-grid correction eliminates all errors at C-points; following this with an effective relaxation on F-points will guarantee a rapidly convergent method [30, Section 2.3]. Due to the A_{ff}^{-1} term in R_{ideal} , it is not practical to form R_{ideal} explicitly. However, AIR appeals to the observation that for upwinded advective discretizations, one can achieve cheap, accurate, and sparse approximations $R \approx R_{\text{ideal}}$.

3.1 Coarsening in space-time

For problems with strong anisotropy or advective components, it is often helpful or even necessary to semi-coarsen along the direction of anisotropy/advection for an effective multigrid method (e.g., [56]). On a high-level, we claim that one of the primary difficulties in applying common (multilevel) PinT schemes to

advective/hyperbolic problems is the separate treatment of temporal and spatial variables. A natural result of this is that coarsening performed separately in space and time is often unable to align with hyperbolic characteristics in space-time. Conversely, by treating space and time all-at-once, it is natural for coarsening to align with characteristics, which provides an important piece of a scalable multilevel method.

Figure 2 demonstrates how classical AMG coarsening [40] applied to a hyperbolic 2d-space/1d-time HDG discretization naturally applies semi-coarsening along the direction of (space-time) characteristics. For clarity, examples are shown in two-dimensional subdomains for the problem described in section 4.2, with plots for the advective field and the corresponding CF-splitting. The velocity fields given in (a) and (b) correspond to CF-splittings in (d) and (e), respectively. Note that for both cases, we largely see stripes of fine and coarse points orthogonal to the flow direction, which is exactly semi-coarsening along the characteristics. Similarly, in (c), note that in the $[0, 0.2] \times [0, 0.2]$ spatial subdomain (for all time), there is effectively no spatial advection, and thus the space-time advective field is only traveling forward in time. Plots (f)–(i) demonstrate an effective semi-coarsening in time, where we mark coarse points on the time levels (see (f) and (i)) and fine points on interior time DOFs (see (g) and (h)).

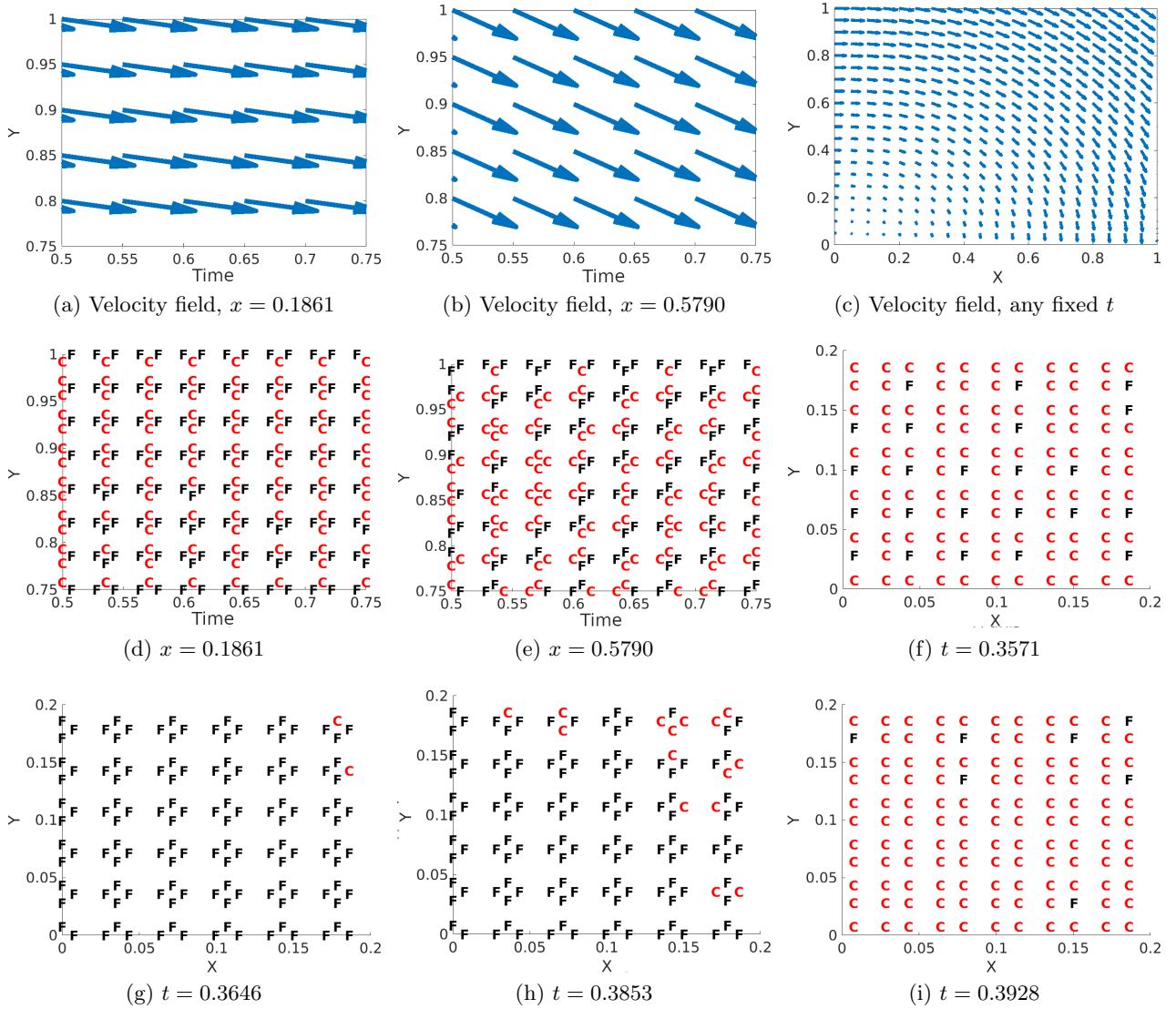


Figure 2: Red points are C-points and black points are F-points for the hyperbolic problem from section 4.2. Distribution of the C- and F- points follow the velocity fields, showing semi-coarsening along characteristics.

3.2 Relaxation and element ordering

Upwinded discontinuous discretizations of linear hyperbolic problems have the benefit that the mesh elements can typically be reordered to be (element) block lower triangular. The corresponding linear system can then be solved directly using a forward solve. Although this is not scalable in parallel (because each process must wait for the previous to finish its solve), it provides an excellent relaxation scheme when each core inverts the subdomain stored on-process. Such a method is commonly used in the transport community to avoid the parallel cost and complexity of a full forward solve, and was shown to provide strong convergence when used with AIR in [19].

Here, we show that an analogous property holds for HDG discretizations of advection (steady or space-time). We do so by noting that the existence of such an ordering is equivalent to proving that the graph of the discretization matrix is acyclic. Assume all mesh elements are convex, let $\{\mathcal{K}_i\}$ denote the set of all n_e elements for a given mesh, and let \mathbb{E} denote the graph of connections between elements, where $\mathbb{E}_{ij} = 1$ if \exists a connection from $\mathcal{K}_i \mapsto \mathcal{K}_j$ with respect to the given velocity field and $\mathbb{E}_{ij} = 0$ otherwise. Let $\{\mathcal{S}_{ij}\}$ denote the set of all n_f outgoing faces, with the subscript \mathcal{S}_{ij} indicating a connection $\mathcal{K}_i \mapsto \mathcal{K}_j \in \mathbb{E}$, and \mathbb{F} denoting the graph of connections between faces. Moreover note that

$$\mathcal{S}_{ij} \mapsto \mathcal{S}_{jk} \quad \text{if and only if} \quad \mathcal{K}_i \mapsto \mathcal{K}_j \text{ and } \mathcal{K}_j \mapsto \mathcal{K}_k. \quad (11)$$

Lemma 3.1. *Suppose \mathbb{E} is a directed acyclic graph, and the elements $\{\mathcal{K}_i\}$ are ordered such that \mathbb{E} is lower triangular. Furthermore, numerate faces \mathcal{S}_{ij} with respect to index i and then j , for example, $\{\mathcal{S}_{01}, \mathcal{S}_{02}, \mathcal{S}_{12}, \mathcal{S}_{23}, \dots\}$. Then, \mathbb{F} is also a directed acyclic graph and lower triangular in this ordering.*

Proof. Because \mathbb{E} is lower triangular, $\nexists \mathcal{K}_i \mapsto \mathcal{K}_j$ if $i > j$. It follows by definition that $i < j$ for all faces \mathcal{S}_{ij} . Now, suppose there exists a path $\mathcal{S}_{ij} \mapsto \mathcal{S}_{jk}$ in \mathbb{F} such that $i > k$. By eq. (11), this is true if and only if $\mathcal{K}_i \mapsto \mathcal{K}_j \mapsto \mathcal{K}_k$. However, this is a contradiction to the assumption of \mathbb{E} being lower triangular. In addition note that by the convexity of elements, \nexists connections $\mathcal{S}_{ij} \mapsto \mathcal{S}_{ik}$, that is, connections between outgoing faces with respect to the velocity field on the same element. Enumerating $\{\mathcal{S}_{ij}\}$ first by index i , then (arbitrarily) by index j as the set of faces $\{\hat{\mathcal{S}}_\ell\}$ implies \nexists path $g_{ij} \in \mathbb{F}$, $g : \hat{\mathcal{S}}_i \mapsto \hat{\mathcal{S}}_j$, such that $i > j$, which completes the proof. \square

Lemma 3.1 is useful in that an ordering can be determined for an on-process block Gauss–Seidel relaxation which exactly inverts the advective component in the case of no cycles in the mesh, where the block size is given by the number of DOFs in a given element face. Such a relaxation scheme is explored numerically in section 4.2.

4 Numerical simulations

This section demonstrates the effectiveness of AIR as a preconditioner for BiCGSTAB to solve the linear system eq. (10), including on moving time-dependent domains (section 4.1), and when applying space-time AMR to an interior front problem (section 4.2). All test cases have been implemented in the Modular Finite Element Method (MFEM) library [2] with solver support from HYPRE [1]. Furthermore, we choose the penalty parameter in eq. (7) as $\alpha = 10p^2$ where p is the order of the polynomial approximation (see, for example [39]). Unless otherwise specified, AIR is constructed with distance-one connections for building R , with strength tolerance 0.3; 1-point interpolation [30]; no pre-relaxation; post-forward-Gauss-Seidel relaxation (on process), first on F-points, followed by all points; Falgout coarsening, with strength tolerance 0.2; and as an acceleration method for BiCGSTAB, applied to the HDG space-time matrix, scaled on the left by the facet block-diagonal inverse. All parallel simulations are run on the LLNL Quartz machine.

4.1 Rotating Gaussian pulse on a time-dependent domain

We first consider the solution of a two-dimensional rotating Gaussian pulse on a time-dependent domain [37]. We set $a = (-4x_2, 4x_1)^T$ and $f = 0$. The boundary and initial conditions are chosen such that the

analytical solution is given by

$$u(t, x_1, x_2) = \frac{\sigma^2}{\sigma^2 + 2\nu t} \exp \left(-\frac{(\tilde{x}_1 - x_{1c})^2 + (\tilde{x}_2 - x_{2c})^2}{2\sigma^2 + 4\nu t} \right), \quad (12)$$

where $\tilde{x}_1 = x_1 \cos(4t) + x_2 \sin(4t)$, $\tilde{x}_2 = -x_1 \sin(4t) + x_2 \cos(4t)$, and $(x_{1c}, x_{2c}) = (-0.2, 0.1)$. Furthermore, we set $\sigma = 0.1$ and consider both a diffusion-dominated case with $\nu = 10^{-2}$ and an advection-dominated case with $\nu = 10^{-6}$. The deformation of the time-dependent domain is based on a transformation of the uniform space-time mesh $(t, x_1^u, x_2^u) \in [0, T] \times [-0.5, 0.5]^2$ given by

$$x_i = x_i^u + A(\tfrac{1}{2} - x_i^u) \sin(2\pi(\tfrac{1}{2} - x_i^* + t)) \quad i = 1, 2, \quad (13)$$

where $(x_1^*, x_2^*) = (x_2^u, x_1^u)$, $A = 0.1$, and T is the final time. We show the solution on the time-dependent domain at different time slices and on the full space-time domain (taking $T = 1$) in fig. 3.

Rates of convergence of the space-time error

In table 1 we compute the rates of convergence of the error in the space-time L^2 -norm, i.e.,

$$\|u - u_h\|_{\mathcal{E}_h} := \left(\int_{\mathcal{E}_h} (u - u_h)^2 d\hat{x} \right)^{1/2}.$$

We compute this error taking $T = 1$ and using linear, quadratic, and cubic polynomial approximations to u . We observe optimal rates of convergence, that is, the error in the space-time L^2 -norm is of order $\mathcal{O}(h^{p+1})$ when using a p -th order polynomial approximation, for both the all-at-once and slab-by-slab discretizations. This conclusion is true for both the advection- and diffusion-dominated problem.

Performance of BiCGSTAB with AIR as preconditioner

This section demonstrates the performance of BiCGSTAB with AIR as a preconditioner in both the advection- and diffusion-dominated regimes. We will use the number of iterations to convergence as the indicator of performance as we know that the setup time and cost of applying AIR per BiCGSTAB iteration are linear with respect to the matrix size, i.e. $\mathcal{O}(N)$ [32, 30]. Hence, the total cost to solve the space-time HDG problem will be linearly dependent on the number of BiCGSTAB iterations. In table 2 we list the total number of BiCGSTAB iterations that are required to reach a relative residual of 10^{-12} in an all-at-once discretization with $T = 1$ and using linear, quadratic, and cubic polynomial approximations to u .

When the problem is close to hyperbolic (when $\nu = 10^{-6}$) we observe perfect scalability, that is, the number of iterations required to converge does not change with the problem size. In the advection-dominated regime, $\nu = 10^{-4}$ and $\nu = 10^{-3}$, the iteration count increases slightly with problem size, but the increase is slow, the iteration counts remain quite low. When more significant diffusion is introduced, $\nu = 10^{-2}$ and $\nu = 10^{-1}$, the iteration count starts to grow more rapidly with increasing problem size. These observations hold for all polynomial degrees considered. It is worth pointing out that for $\nu = 10^{-2}$ and $\nu = 10^{-1}$, using a classical P^TAP AMG approach rather than AIR did result in lower iteration counts (not shown), however, the total time to solution remained notably longer than that of AIR, likely due to denser coarse-grid matrices.

From the above observations, we may conclude that BiCGSTAB with AIR as the preconditioner is an excellent iterative solver for the solution of all-at-once space-time HDG discretizations of the advection-diffusion problem in the advection-dominated regime. Unsurprisingly, the solver is suboptimal in the diffusion-dominated regime. To see why, note that we may write eq. (4a) as

$$\hat{a} \cdot \hat{\nabla} u - \hat{\nabla} \cdot (\hat{\nu} \hat{\nabla} u) = f \quad \text{in } \mathcal{E}_h,$$

where $\hat{\nu} = \text{diag}(0, \nu, \nu)$ (note that there is no diffusion in the time direction). This is a “steady” advection-diffusion problem in $(d + 1)$ -dimensional space-time with completely *anisotropic* diffusion in d dimensions

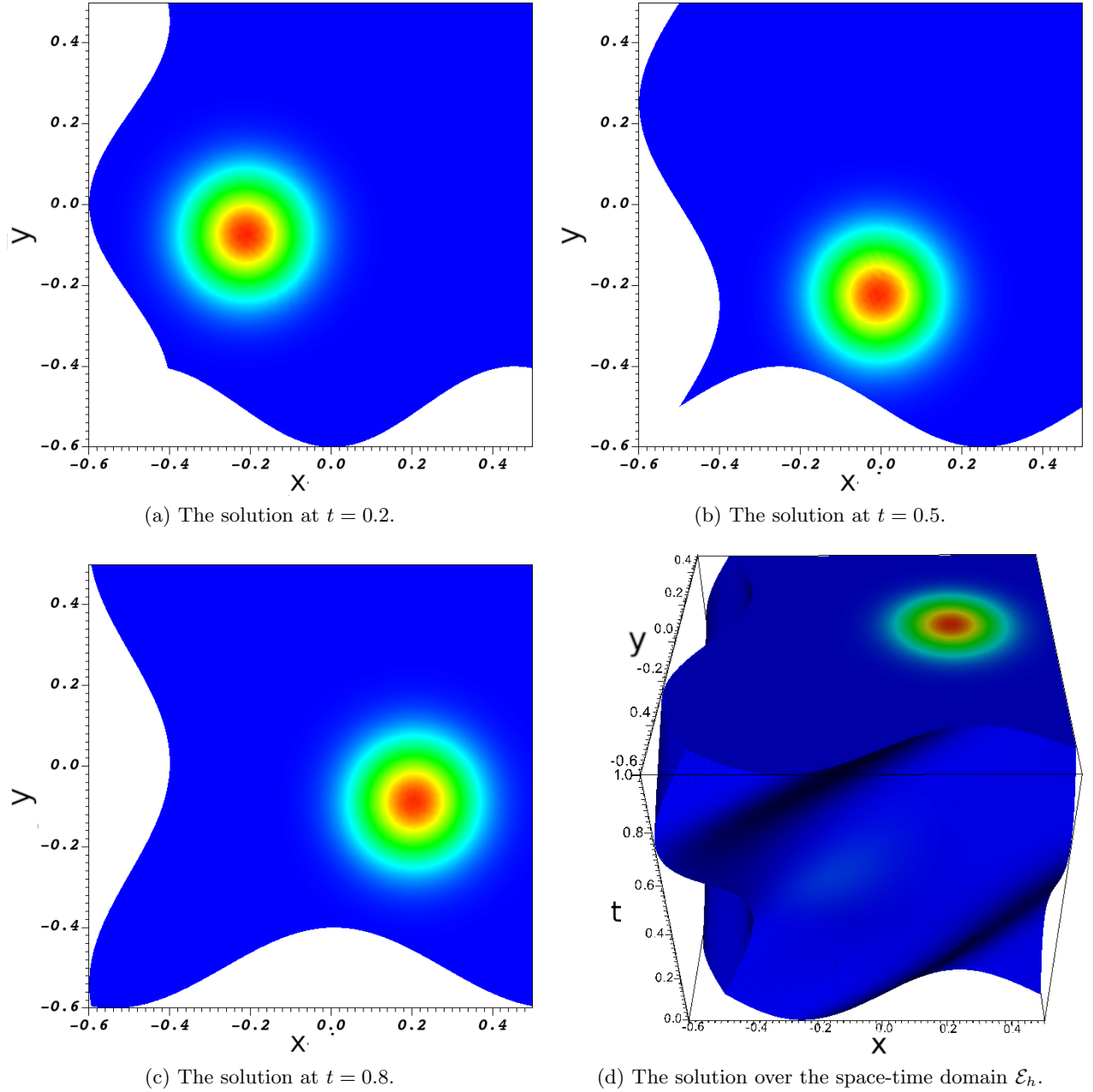


Figure 3: The solution of the rotating Gaussian pulse test case as described in section 4.1 at different time slices and on the full space-time domain when $\nu = 10^{-6}$.

and advection in one dimension. Problems with anisotropic diffusion are known to pose a challenge to multilevel solvers (see, for example, [44] for a literature review on the challenges of using multilevel solvers for problems with anisotropic diffusion). Robust solvers for the mixed regime of advection and strongly anisotropic diffusion are ongoing work.

Remark 4.1 (Stopping tolerance). *Our main goal is to test the performance of BiCGSTAB with AIR as a preconditioner. For this reason, we chose the stopping criteria for BiCGSTAB to be a relative residual of 10^{-12} . In practice, however, the stopping tolerance need not be chosen this small (see, for example [13, pages 73, 77–79]). We demonstrate this also in table 3 where, for the case $p = 2$ for a problem with 272,448 degrees of freedom. We note that the error in the space-time L_2 -norm does not improve after the first full BiCGSTAB iteration although it takes 8 iterations to reach a relative residual of 10^{-12} (see table 2).*

Table 1: Error in the space-time L^2 -norm and rate of convergence of a space-time HDG discretization of the advection-diffusion problem described in section 4.1, with $T = 1$.

Slab-by-slab								
ν	Slabs	Elements per slab	$p = 1$		$p = 2$		$p = 3$	
			Error	Rate	Error	Rate	Error	Rate
10^{-2}	8	384	1.1e-2	-	2.9e-3	-	8.4e-4	-
	16	1,536	3.4e-3	1.7	4.7e-4	2.6	5.8e-5	3.9
	32	6,144	8.4e-4	2.0	5.9e-5	3.0	3.7e-6	4.0
	64	24,576	2.1e-4	2.0	7.4e-6	3.0	2.3e-7	4.0
10^{-6}	8	384	1.9e-2	-	5.3e-3	-	1.3e-3	-
	16	1,536	6.1e-3	1.6	8.5e-4	2.7	1.3e-4	3.4
	32	6,144	1.6e-3	2.0	1.1e-4	3.0	9.0e-6	3.8
	64	24,576	3.8e-4	2.0	1.4e-5	3.0	5.9e-7	3.9
All-at-once								
ν	Elements	$p = 1$		$p = 2$		$p = 3$		
		Error	Rate	Error	Rate	Error	Rate	
10^{-2}	2,760	2.0e-2	-	6.0e-3	-	1.7e-3	-	
	22,080	5.8e-3	1.8	8.2e-4	2.9	1.2e-4	3.8	
	176,640	1.3e-3	2.1	9.5e-5	3.1	7.5e-6	4.0	
	1,413,120	3.0e-4	2.1	1.2e-5	3.1	4.6e-7	4.0	
10^{-6}	2,760	5.5e-2	-	2.1e-2	-	8.9e-3	-	
	22,080	2.0e-2	1.4	3.6e-3	2.6	7.2e-4	3.6	
	176,640	5.1e-3	2.0	3.8e-4	3.2	4.5e-5	4.0	
	1,413,120	1.0e-3	2.3	4.3e-5	3.2	2.6e-6	4.1	

Remark 4.2 (GMRES and other Krylov). *In this section we considered the performance of BiCGSTAB with AIR as a preconditioner. Of course, we may replace BiCGSTAB with any other iterative method for non-symmetric systems of linear equations. GMRES performed equally well in most cases; however, there were several examples that stalled significantly upon GMRES restart, and which also required a moderately high number of iterations to convergence, limiting the use of full-memory GMRES. In our tests, BiCGSTAB has appeared to be slightly more robust and, thus, is used for all numerical tests presented here.*

Scalability and parallel-in-time on moving domains

The current paradigm in scientific computing is to use multiple computing units simultaneously to lower runtime. Hence, the scalability of an algorithm is an important measure of performance. Ideally, the runtime should be inversely proportional to the number of computing units. Unfortunately, this is not always achievable due to limited fast access memory (caches), limited memory bandwidth, and inter-process and inter-node communication. One advantage of the all-at-once space-time approach over the slab-by-slab space-time approach is the better communication to computation ratio. This is because it is possible to parallelize both in space and time simultaneously, as opposed to the standard parallel-in-time approach of treating space and time separately.

To test the scalability of BiCGSTAB with AIR as a preconditioner applied to the space-time HDG discretization, we will measure the total wall-clock time spent on solving the rotating Gaussian pulse problem discussed at the beginning of this section. For this, we consider a final time of $T = 16$, we consider both an advection- ($\nu = 10^{-6}$) and a diffusion-dominated ($\nu = 10^{-2}$) problem, and we consider both an all-at-once

Table 2: The number of BiCGSTAB iterations (with AIR as the preconditioner) required to reach a relative residual of 10^{-12} for the test case described in section 4.1 with $T = 1$. The stopping tolerance was not reached within 5000 iterations if a value is missing.

$p = 1$					
DOFs	ν				
	10^{-6}	10^{-4}	10^{-3}	10^{-2}	10^{-1}
17,496	7	7	7	8	12
136,224	8	7	8	10	17
1,074,816	8	8	10	13	54
8,538,624	8	9	12	18	-

$p = 2$					
DOFs	ν				
	10^{-6}	10^{-4}	10^{-3}	10^{-2}	10^{-1}
34,992	11	8	9	11	19
272,448	8	9	10	14	30
2,149,632	9	11	13	18	46
17,077,248	9	14	15	30	83

$p = 3$					
DOFs	ν				
	10^{-6}	10^{-4}	10^{-3}	10^{-2}	10^{-1}
58,320	9	8	10	14	26
454,080	9	11	12	18	38
3,582,720	9	13	15	25	73
28,462,080	10	17	18	46	144

Table 3: Error in the space-time L_2 -norm as a function of BiCGSTAB iteration number for the test case from table 2. We use a quadratic ($p = 2$) polynomial approximation and the linear system has 272,448 degrees of freedom. The preconditioned residual presented in the table is the residual of the full-step.

Iteration Number	Preconditioned Residual	$\ u - u_h\ _{L_2(\mathcal{E}_h)}$
0	2.5e-4	1.6e-3
1	8.4e-6	3.6e-3
2	1.0e-6	3.6e-3
3	6.1e-9	3.6e-3
4	1.6e-10	3.6e-3

and a slab-by-slab discretization. For the all-at-once discretization, we consider two unstructured space-time meshes; the coarse mesh consists of 45576 tetrahedra and the fine mesh consists of 364608 tetrahedra. For the slab-by-slab approach, we consider a coarse mesh in which the space-time domain is divided into 128 space-time slabs and each slab consists of 384 tetrahedra. The fine slab-by-slab mesh consists of 256 slabs and each slab consists of 1536 tetrahedra. Note that the slab-by-slab meshes were created to have a similar number of tetrahedra as the all-at-once space-time meshes.

The total wall-clock times we measure are the combination of time spent on the following four stages: setup, assembly, solving, and reconstruction. During the setup stage, the mesh is read from a file and refined sequentially and finite element spaces and linear and bi-linear forms are created. We remark that this stage is not parallelizable and it affects the speedup we obtain. The assembly stage contains the computation of elemental matrices, computation of elemental Schur complements, and the assembly of the global linear system eq. (10). This stage is almost embarrassingly parallel. The next stage is the solve stage in which the global linear system is solved using BiCGSTAB with AIR as the preconditioner. This stage is weakly scalable. Finally, the element solution $U = A^{-1}(F - BA)$ is reconstructed in the reconstruction stage (see section 2.5). This step, in theory, does not require any communication as it can be done completely locally.

Parallel speedup in a strong-scaling sense for each combination of mesh resolution and diffusion coefficient is shown in fig. 4. We see that, in all cases, the all-at-once approach is the best algorithm sequentially. Hence, the speedups are calculated relative to the sequential timing of the solutions using all-at-once approach for different order of approximations. The best speedup we achieve at 256 processes is slightly more than 100, and just less than 50% efficiency. This can be mostly attributed to the sequential nature of the setup stage, for example, it takes up to 10% of wall-clock time spent for large problems solved with many (64-256) cores. In addition to this, there is a significant loss of scalability during the solve stage, which is largely due to the algorithm becoming communication bound and thereby less efficient in parallel. For example, the speedup observed on the fine mesh at 256 processes is close to $2\times$ larger than that observed on the coarse mesh. Hence, for larger problems, we expect better speedup with the primary bottleneck being the setup stage. It is worth pointing out that a number of recent works have developed architecture-aware communication algorithms for sparse matrix-vector operations and AMG that can significantly improve scalability in the communication-bound regime (e.g., [4, 5]), but we do not exploit such methods here.

fig. 5 plots the relative speedup of the all-at-once approach to the slab approach with respect to wall-clock time, that is, $\text{Time}_{\text{all-at-once}}(n)/\text{Time}_{\text{slab-by-slab}}(n)$. We see that, generally, the all-at-once approach is 20% to 50% faster than the slab-by-slab approach, although in some cases it is up to $2\times$ faster. Note that this comparison is imperfect, and an accurate measure of speedup is nuanced – for example, the slab mesh here has roughly 8% more elements than the all-at-once mesh; however, the slab mesh is also structured in time, while the all-at-once mesh is fully unstructured in space and time, which can degrade performance of multigrid solvers on a fine-grained/memory-access level. They also differ algorithmically; for example, the all-at-once approach does one setup phase for AIR, followed by the solve phase, while using the slab-by-slab approach requires rebuilding the solver each time step. In general, we do not try to isolate where the speedup comes from in this paper. Rather, we highlight here that by using AIR as a full space-time solver, we are able to see speedups over sequential time stepping for low core counts, a property that is not shared by most parallel-in-time schemes.

4.2 Moving internal layer problem

We now consider the moving internal layer problem proposed in [10]. We solve eq. (4) on the unit cube space-time domain $(\mathcal{E}_h = [0, 1]^3)$ with $a = (x_2, -x_1)^T$, $f = 0$, and with $\nu = 0$ (the hyperbolic limit). We impose a Neumann boundary at $t = 0$, on which we set $g_N = 0$, and an outflow boundary at the final time $t = 1$. On the boundary $x_2 = 0$ we set $g_D = 1$ and we set $g_D = 0$ on the remaining boundaries. For the time interval of interest, the exact solution is given by

$$u(t, x_1, x_2) = \begin{cases} 1 & \text{when } \|(x_1, x_2)\|_2 < 1 \text{ and } \text{atan2}(x_2, x_1) > \pi/2 - t, \\ 0 & \text{otherwise,} \end{cases}$$

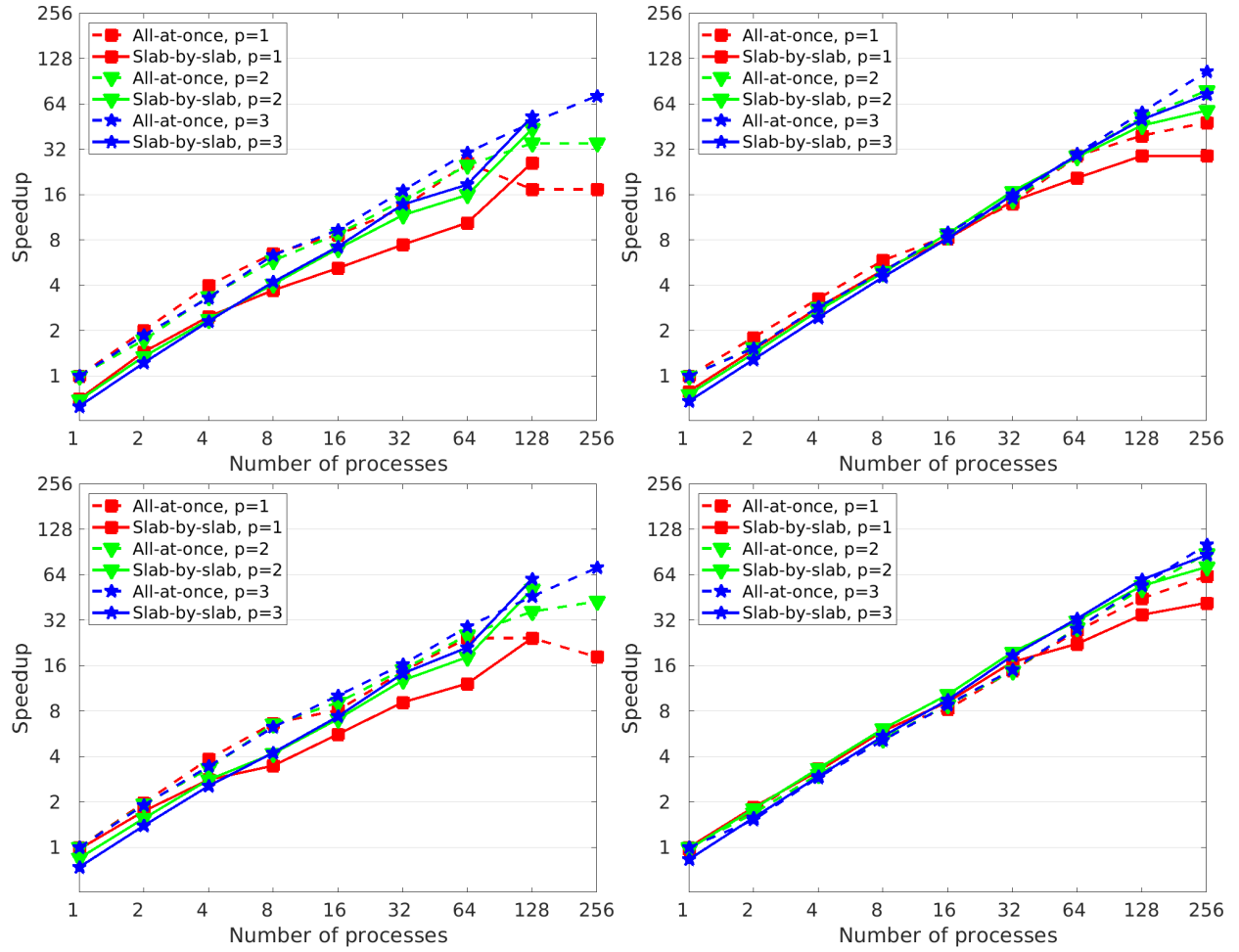


Figure 4: Parallel scalability. Top left: $\nu = 10^{-6}$, coarse mesh, top right: $\nu = 10^{-6}$, fine mesh, bottom left: $\nu = 10^{-2}$, coarse mesh, bottom right: $\nu = 10^{-2}$, fine mesh

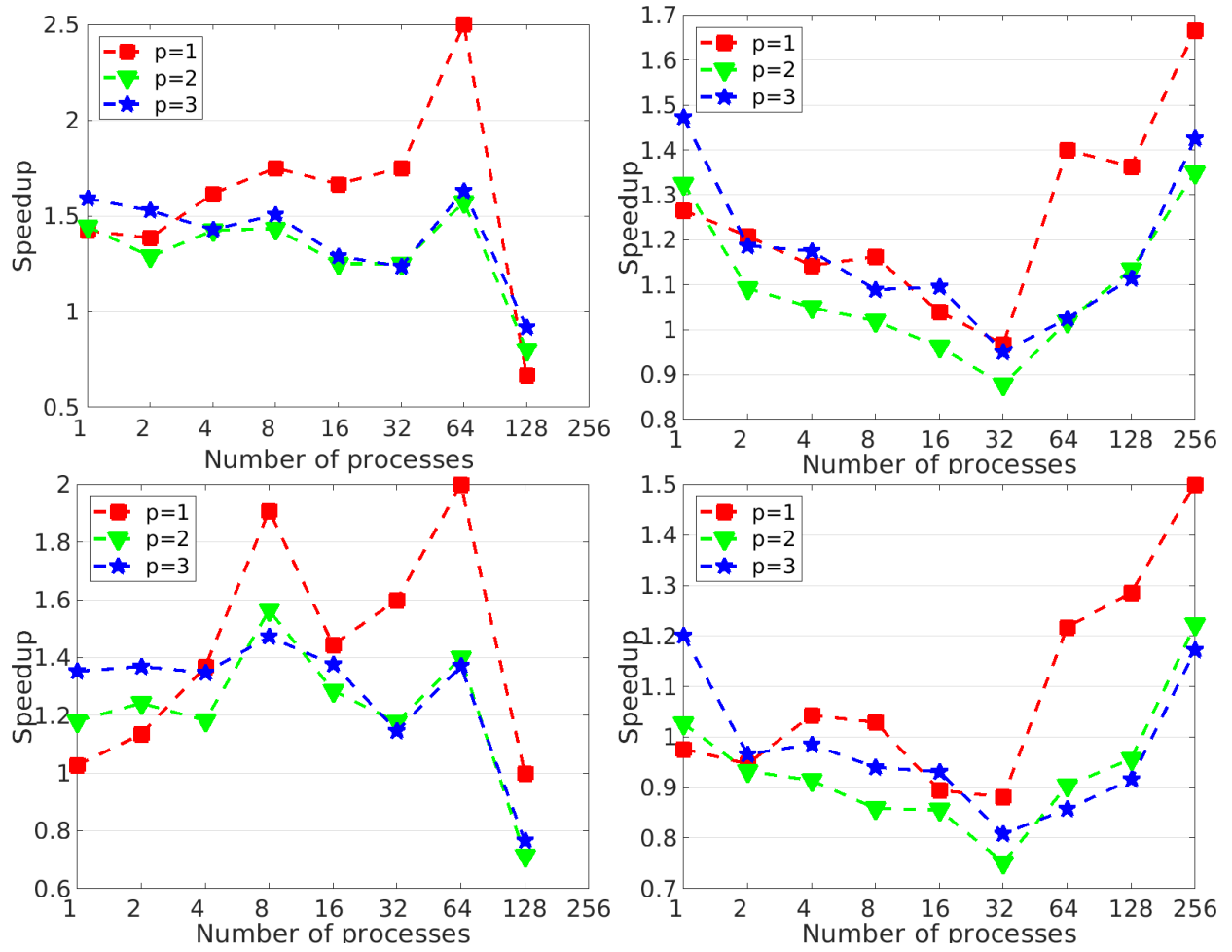


Figure 5: Relative speedup of all-at-once approach against slab-by-slab approach. Top left: $\nu = 10^{-6}$, coarse mesh, top right: $\nu = 10^{-6}$, fine mesh, bottom left: $\nu = 10^{-2}$, coarse mesh, bottom right: $\nu = 10^{-2}$, fine mesh

which describes a front that rotates around the origin as time evolves.

Space-time adaptive mesh refinement

To efficiently solve this problem, we use space-time adaptive mesh refinement (AMR) in an all-at-once discretization, where we refine locally in both space and time. The Zienkiewicz–Zhu (ZZ) error estimator [58, 59, 60] is used to mark space-time elements that need to be refined. Although the ZZ error estimator is not theoretically efficient or reliable for many problems, it is often used heuristically in adaptive finite element codes due to its simplicity, low computational cost, and wide availability. See fig. 6 for a plot of the mesh and the solution at two different time slices. A plot of the adaptively refined mesh in space-time is given in fig. 7.

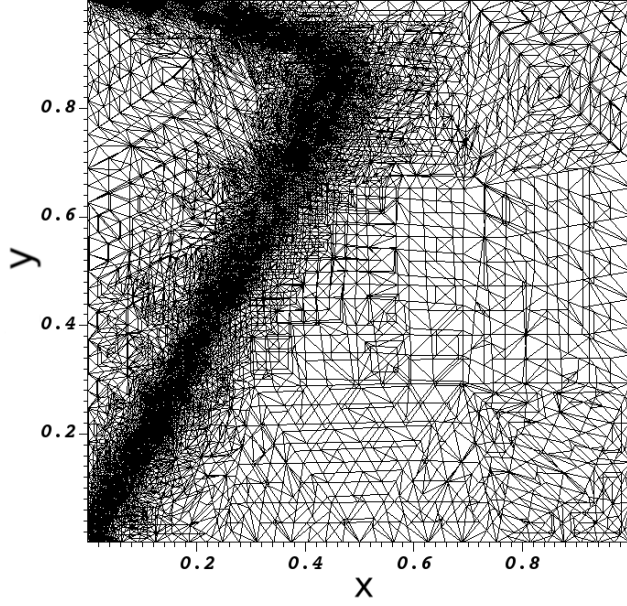
In fig. 8 we compare the convergence of the error in the space-time L^2 -norm using space-time AMR to using uniformly refined meshes. Let N be the total number of globally coupled DOFs. We see that the error on uniform meshes is approximately $\mathcal{O}(N^{-1/9})$ while the error on the space-time AMR meshes is approximately $\mathcal{O}(N^{-1/6})$, i.e., we obtain faster convergence using space-time AMR than when using uniformly refined meshes. We remark that the error when using an efficient and reliable error estimator for this problem is expected to be $\mathcal{O}(N^{-1/3})$ (see, for example, [7] for the analysis of an a posteriori error estimator for a DG discretization of the steady advection equation). However, we are not aware of any efficient and reliable error estimators for space-time HDG discretizations of the time-dependent advection equation.

Performance of AIR and on-process solves

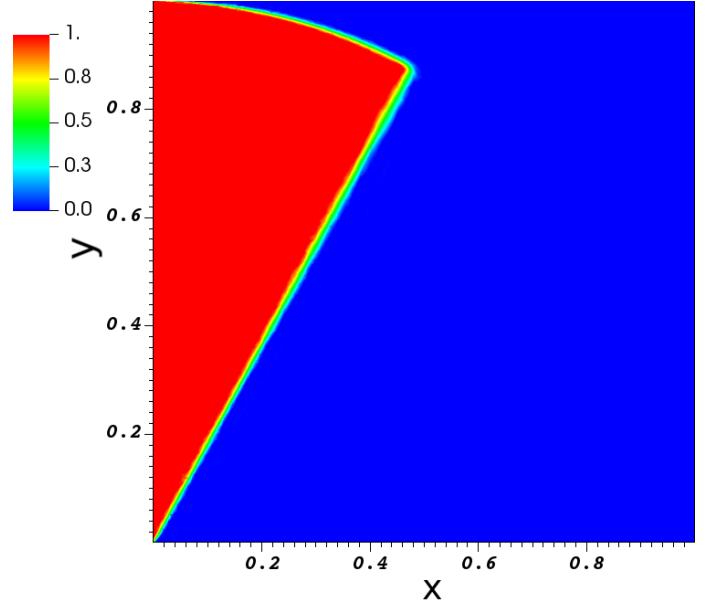
Last, we consider the performance of BiCGSTAB with AIR as a preconditioner within the context of space-time AMR, and demonstrate the application of lemma 3.1. It is well known that upwind DG discretizations of advection on convex elements yield matrices that are block triangular in some element ordering. This can serve as a robust on-process relaxation routine, where the triangular element ordering is obtained and an ordered block Gauss–Seidel exactly inverts the on-process subdomain [19]. AIR also relies, in some sense, on having a matrix with dominant lower triangular structure, where it can be shown that triangular structure allows for a good approximation to ideal restriction [30]. Although HDG discretizations are not always thought of as block linear systems in the same way that DG discretizations are, Lemma 3.1 proves that by treating DOFs on a given facet as a block in the matrix, an analogous result holds, that is, the matrix is block lower triangular in some ordering. With AIR preconditioning, the block structure can be accounted for by using a block implementation of AIR (e.g., [32]) coupled with block relaxation or, in the advection-dominated regime, scaling on the left by the block-diagonal inverse, wherein the scaled matrix is then scalar lower triangular.

Figure 9 demonstrates each of these points in practice, applying AIR to a succession of adaptively refined space-time problems with various relaxation and block inverse strategies. The number of DOFs on the x-axis corresponds to successive levels of adaptive space-time mesh refinement (with correspondingly larger number of DOFs). First, note that accounting for the block structure in the matrix is important for scalable convergence at larger problem sizes. Not scaling by the block inverse (“No Block Inv”) can lead to an increase in iteration count by more than $3\times$ for the largest problem size, and likely worse as DOFs further increase. On the other hand, after applying the block inverse scaling, even pointwise Jacobi relaxation yields near perfectly scalable convergence. Furthermore, because we are considering a hyperbolic equation with cycle-free space-time velocity field $\hat{a} = (1, x_2, -x_1)^T$, from lemma 3.1 the scaled matrix is lower triangular. A topological sort of the on-process matrix yields the triangular ordering, and an ordered Gauss–Seidel relaxation then exactly inverts the on-process block. Simulations in fig. 9 are run on 128 cores, and we see that with an on-process solve as relaxation, the number of iterations required to converge is half of the second-best relaxation method we tested, forward Gauss–Seidel (although both are still quite good).¹

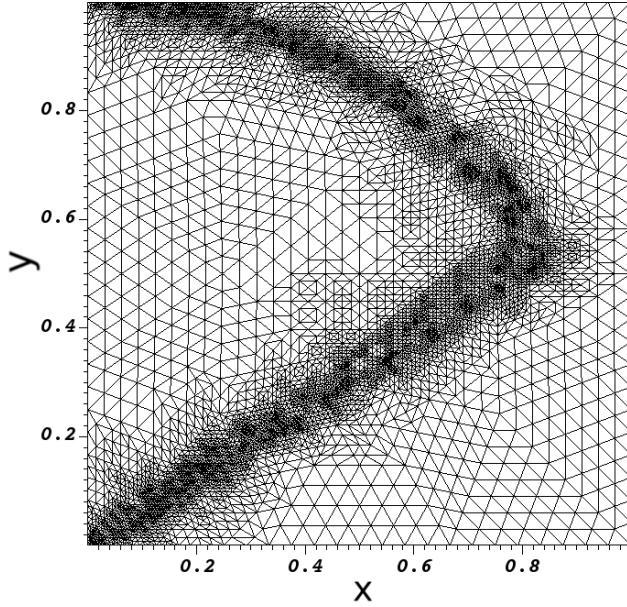
¹Note that the moving domain considered in section 4.1 introduces cycles in the matrix-graph, and the resulting matrix is not necessarily block triangular. However, cycle-breaking strategies such as used in [20] for DG transport simulations on curvilinear



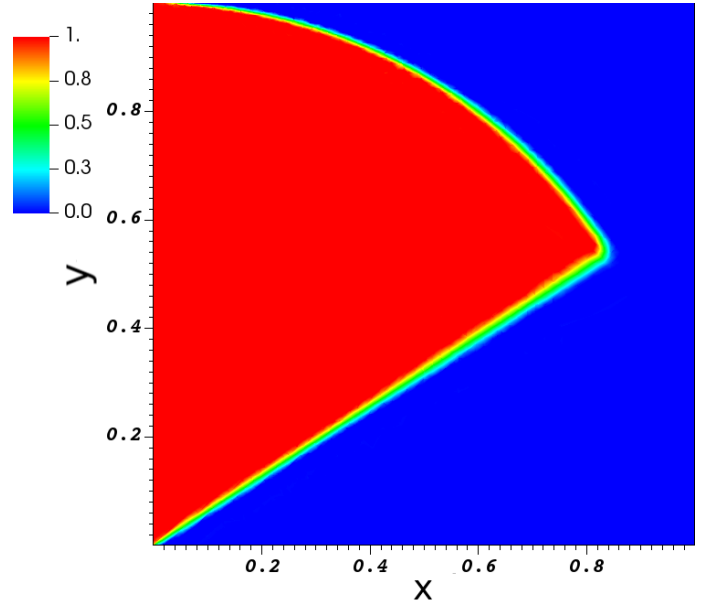
(a) Mesh slice at $t = 0.5$



(b) Solution slice at $t = 0.5$



(c) Mesh slice at $t = 1$



(d) Solution slice at $t = 1$

Figure 6: The numerical solution to the interior layer problem at two different time slices. The non-triangular polygons in the top left figure are because we are slicing the space-time mesh at $t = 0.5$; we are cutting through space-time tetrahedra.

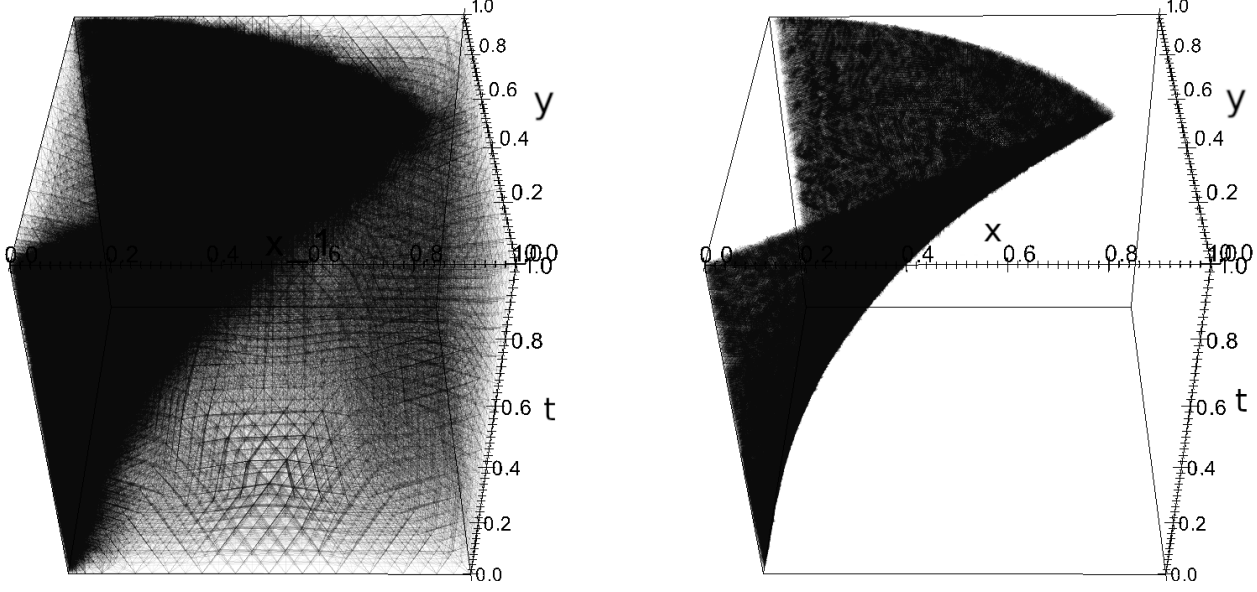


Figure 7: Left: the space-time AMR mesh obtained using the ZZ error estimator for the test case described in section 4.2. Right: only the elements below the median element size are shown. Note that the mesh is refined along the space-time interior layer.

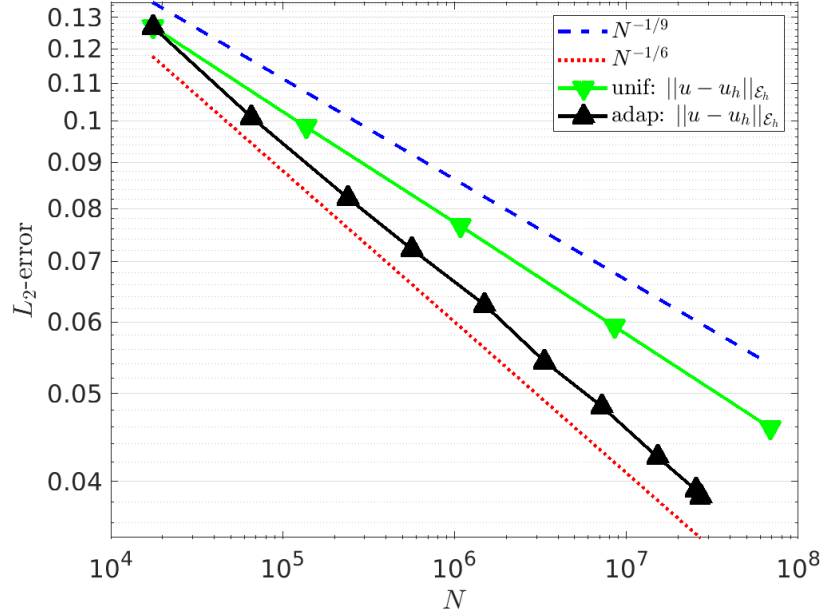


Figure 8: We compare the convergence of the error in the space-time L^2 -norm using space-time AMR to using uniformly refined space-time meshes. The test case is described in section 4.2. Here N is the total number of globally coupled DOFs.

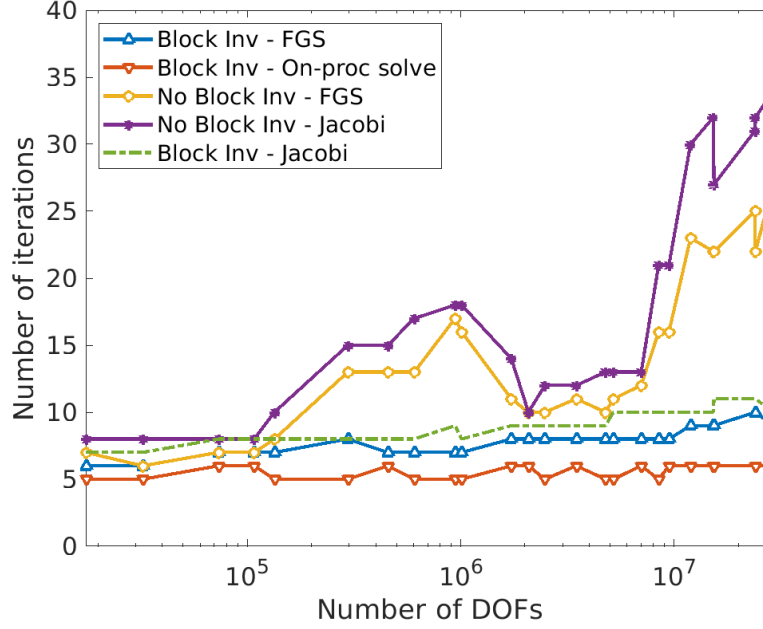


Figure 9: A comparison of the number of BiCGSTAB iterations to convergence using AIR as preconditioner with different relaxation strategies. We plot the number of iterations against the number of globally coupled DOFs at different levels of refinement within the AMR algorithm.

Remark 4.3 (Relation to PinT). *It is worth pointing out the relation of the on-process solve to PinT methods. In MGRiT and Parareal, the relaxation scheme corresponds to solving the time-propagation problem between F -time-points. If you assign one F -point per process, this is solving the time-propagation problem exactly on process and is coupled with a coarsening in time. Similar to the discussion in section 3.1 here, we actually solve the space-time problem exactly along the characteristics on each process, which is then coupled with a coarsening that aligns with the characteristics (see fig. 2). Again, we believe this more holistic treatment of space and time is what allows for perfectly scalable parallel-in-time convergence on hyperbolic problems.*

5 Conclusions

AIR algebraic multigrid is known to be a robust preconditioner for discretizations of steady advection-dominated advection-diffusion problems. This paper was motivated by the question whether AIR AMG is robust as an all-at-once solver for space-time HDG discretizations of time-dependent advection-diffusion problems, since such problems can be seen as “steady” advection-diffusion problems in $(d + 1)$ -dimensions. By numerical examples, we have indeed demonstrated that AIR provides fast, effective, and scalable preconditioning for space-time discretizations of advection-dominated problems, including robust convergence on space-time AMR and moving, time-dependent domains.

Advection-dominated problems are notoriously difficult for parallel-in-time methods, motivating a number of efforts to develop specialized techniques that can handle advection on coarse time-grids (e.g., [11, 9]). Here, we claim that the best way to provide time parallelism for hyperbolic problems is by treating space and time *together*. In particular, a critical component in multigrid methods is constructing an effective coarse grid. By applying AIR all-at-once to a space-time discretization, coarsening is able to align with hyperbolic characteristics in space-time and provide a coarse-grid that naturally captures these characteristics.

meshes can find a “good” ordering and provide comparable performance as a direct on-process solve when coupled with the larger AIR algorithm.

Moreover, we proved that for purely hyperbolic problems, the space-time HDG discretization on convex elements is block triangular in some ordering. Using this ordering, a relaxation scheme can be designed that exactly solves along the characteristics on-process, complementing the coarse-grid alignment. Classical parallel-in-time multigrid methods that coarsen in space and time separately are typically unable to align with hyperbolic characteristics, often resulting in slow convergence or divergence for time-dependent advection-dominated problems.

Acknowledgments

Los Alamos National Laboratory report number LA-UR-20-28396. This research was enabled in part by the support provided by Sharcnet (<https://www.sharcnet.ca/>) and Compute Canada (<https://www.computeCanada.ca>). We are furthermore grateful for the computing resources provided by the Math Faculty Computing Facility at the University of Waterloo (<https://uwaterloo.ca/math-faculty-computing-facility/>).

References

- [1] *hypr: High performance preconditioners*. <http://www.llnl.gov/casc/hypr>, 2020.
- [2] *MFEM: Modular finite element methods*. mfem.org, 2020.
- [3] V. R. AMBATI AND O. BOKHOVE, *Space-time discontinuous Galerkin discretization of rotating shallow water equations*, J. Comput. Phys., 225 (2007), pp. 1233–1261, <https://doi.org/10.1016/j.jcp.2007.01.036>.
- [4] A. BIENZ, W. D. GROPP, AND L. N. OLSON, *Node aware sparse matrix-vector multiplication*, J. Parallel Distr. Com., 130 (2019), pp. 166–178, <https://doi.org/10.1016/j.jpdc.2019.03.016>.
- [5] A. BIENZ, W. D. GROPP, AND L. N. OLSON, *Reducing communication in algebraic multigrid with multi-step node aware communication*, Int. J. High Perform. C., (2020), p. 1094342020925535, <https://doi.org/10.1177/1094342020925535>.
- [6] M. BREZINA, T. A. MANTEUFFEL, S. F. MCCORMICK, J. W. RUGE, AND G. SANDERS, *Towards Adaptive Smoothed Aggregation (α SA) for Nonsymmetric Problems*, SIAM J. Sci. Comput., 32 (2010), pp. 14–39, <https://doi.org/10.1137/080727336>.
- [7] E. BURMAN, *A posteriori error estimation for interior penalty finite element approximations of the advection-reaction equation*, SIAM J. Numer. Anal., 47 (2009), pp. 3584–3607, <https://doi.org/10.1137/080733899>.
- [8] B. COCKBURN, J. GOPALAKRISHNAN, AND R. LAZAROV, *Unified hybridization of discontinuous Galerkin, mixed, and continuous Galerkin methods for second order elliptic problems*, SIAM J. Numer. Anal., 47 (2009), pp. 1319–1365, <https://doi.org/10.1137/070706616>.
- [9] X. DAI AND Y. MADAY, *Stable parareal in time method for first-and second-order hyperbolic systems*, SIAM J. Sci. Comput., 35 (2013), pp. A52–A78, <https://doi.org/10.1137/110861002>.
- [10] J. DE FRUTOS, B. GARCÍA-ARCHILLA, V. JOHN, AND J. NOVO, *An adaptive SUPG method for evolutionary convection-diffusion equations*, Comput. Methods Appl. Mech. Engrg., 273 (2014), pp. 219–237, <https://doi.org/10.1016/j.cma.2014.01.022>.
- [11] H. DE STERCK, R. D. FALGOUT, S. FRIEDHOFF, O. A. KRZYSIK, AND S. P. MACLACHLAN, *Optimizing MGRIT and parareal coarse-grid operators for linear advection*, arXiv preprint arXiv:1910.03726, (2019).

- [12] H. DE STERCK, S. FRIEDHOFF, A. J. HOWSE, AND S. P. MACLACHLAN, *Convergence analysis for parallel-in-time solution of hyperbolic systems*, Numer. Linear Algebra Appl., 27 (2020), p. e2271, <https://doi.org/10.1002/nla.2271>.
- [13] H. C. ELMAN, D. J. SILVESTER, AND A. J. WATHEN, *Finite elements and fast iterative solvers: with applications in incompressible fluid dynamics*, Oxford University Press, USA, 2nd ed., 2014.
- [14] R. D. FALGOUT, S. FRIEDHOFF, T. V. KOLEV, S. P. MACLACHLAN, AND J. B. SCHRODER, *Parallel time integration with multigrid*, SIAM J. Sci. Comput., 36 (2014), pp. C635–C661, <https://doi.org/10.1137/130944230>.
- [15] R. D. FALGOUT, S. FRIEDHOFF, T. V. KOLEV, S. P. MACLACHLAN, J. B. SCHRODER, AND S. VANDEWALLE, *Multigrid methods with space-time concurrency*, Comput. Vis. Sci., 18 (2017), pp. 123–143, <https://doi.org/10.1007/s00791-017-0283-9>.
- [16] S. FRIEDHOFF AND B. S. SOUTHWORTH, *On “optimal” h -independent convergence of parareal and multigrid-reduction-in-time using Runge-Kutta time integration*, Numer. Linear Algebra Appl., (2020), p. e2301, <https://doi.org/10.1002/nla.2301>.
- [17] M. J. GANDER AND M. NEUMULLER, *Analysis of a new space-time parallel multigrid algorithm for parabolic problems*, SIAM J. Sci. Comput., 38 (2016), pp. A2173–A2208, <https://doi.org/10.1137/15M1046605>.
- [18] J. GOPALAKRISHNAN, M. NEUMÜLLER, AND P. S. VASSILEVSKI, *The auxiliary space preconditioner for the de Rham complex*, SIAM J. Numer. Anal., 56 (2018), pp. 3196–3218, <https://doi.org/10.1137/17M1153376>.
- [19] J. HANOPHY, B. S. SOUTHWORTH, R. LI, T. MANTEUFFEL, AND J. MOREL, *Parallel approximate ideal restriction multigrid for solving the SN transport equations*, Nucl. Sci. Eng., (2020), pp. 1–20, <https://doi.org/10.1080/00295639.2020.1747263>.
- [20] T. HAUT, P. MAGINOT, V. TOMOV, B. SOUTHWORTH, T. BRUNNER, AND T. BAILEY, *An efficient sweep-based solver for the SN equations on high-order meshes*, Nucl. Sci. Eng., 193 (2019), pp. 746–759, <https://doi.org/10.1080/00295639.2018.1562778>.
- [21] G. HORTON AND S. VANDEWALLE, *A space-time multigrid method for parabolic partial differential equations*, SIAM J. Sci. Comput., 16 (1995), pp. 848–864, <https://doi.org/10.1137/0916050>.
- [22] T. L. HORVÁTH AND S. RHEBERGEN, *A locally conservative and energy-stable finite element method for the Navier–Stokes problem on time-dependent domains*, Int. J. Numer. Meth. Fluids, 89 (2019), pp. 519–532, <https://doi.org/10.1002/fld.4707>.
- [23] T. L. HORVÁTH AND S. RHEBERGEN, *An exactly mass conserving space-time embedded-hybridized discontinuous Galerkin method for the Navier–Stokes equations on moving domains*, J. Comput. Phys., 417 (2020), <https://doi.org/10.1016/j.jcp.2020.109577>.
- [24] B. HÜBNER, E. WALHORN, AND D. DINKLER, *A monolithic approach to fluid-structure interaction using space-time finite elements*, Comput. Methods Appl. Mech. Engrg., 193 (2004), pp. 2087–2104, <https://doi.org/10.1016/j.cma.2004.01.024>.
- [25] P. JAMET, *Galerkin-type approximations which are discontinuous in time for parabolic equations in a variable domain*, SIAM J. Numer. Anal., 15 (1978), pp. 912–928, <https://doi.org/10.1137/0715059>.
- [26] K. L. A. KIRK, T. L. HORVATH, A. CESMELIOGLU, AND S. RHEBERGEN, *Analysis of a space-time hybridizable discontinuous Galerkin method for the advection-diffusion problem on time-dependent domains*, SIAM J. Numer. Anal., 57 (2029), pp. 1677–1696, <https://doi.org/10.1137/18M1202049>.

- [27] M. LESOINNE AND C. FARHAT, *Geometric conservation laws for flow problems with moving boundaries and deformable meshes, and their impact on aeroelastic computations*, Comput. Methods. Appl. Mech. Engrg., 134 (1996), pp. 71–90, [https://doi.org/10.1016/0045-7825\(96\)01028-6](https://doi.org/10.1016/0045-7825(96)01028-6).
- [28] J. L. LIONS, Y. MADAY, AND G. TURINICI, *Résolution d'EDP par un schéma en temps pararéel*, C. R. Acad. Sci. Paris Sér. I Math, 332 (2001), pp. 661–668, [https://doi.org/10.1016/S0764-4442\(00\)01793-6](https://doi.org/10.1016/S0764-4442(00)01793-6).
- [29] C. MAKRIDAKIS AND R. H. NOCHETTO, *A posteriori error analysis for higher order dissipative methods for evolution problems*, Numer. Math. (Heidelb), 104 (2006), pp. 489–514, <https://doi.org/10.1007/s00211-006-0013-6>.
- [30] T. A. MANTEUFFEL, S. MÜNZENMAIER, J. RUGE, AND B. S. SOUTHWORTH, *Nonsymmetric reduction-based algebraic multigrid*, SIAM J. Sci. Comput., 41 (2019), pp. S242–S268, <https://doi.org/10.1137/18M1193761>.
- [31] T. A. MANTEUFFEL, L. N. OLSON, J. B. SCHRODER, AND B. S. SOUTHWORTH, *A root-node based algebraic multigrid method*, SIAM J. Sci. Comput., 39 (2017), pp. S723–S756, <https://doi.org/10.1137/16M1082706>.
- [32] T. A. MANTEUFFEL, J. RUGE, AND B. S. SOUTHWORTH, *Nonsymmetric algebraic multigrid based on local approximate ideal restriction (lAIR)*, SIAM J. Sci. Comput., 40 (2018), pp. A4105–A4130, <https://doi.org/10.1137/17M1144350>.
- [33] A. MASUD AND T. HUGHES, *A space-time Galerkin/least-squares finite element formulation of the Navier–Stokes equations for moving domain problems*, Comput. Methods Appl. Mech. Engrg., 146 (1997), pp. 91–126, [https://doi.org/10.1016/S0045-7825\(96\)01222-4](https://doi.org/10.1016/S0045-7825(96)01222-4).
- [34] Y. NOTAY, *Aggregation-based algebraic multigrid for convection-diffusion equations*, SIAM J. Sci. Comput., 34 (2012), pp. A2288–A2316, <https://doi.org/10.1137/110835347>.
- [35] P.-O. PERSSON, J. BONET, AND J. PERAIRE, *Discontinuous Galerkin solution of the Navier–Stokes equations on deformable domains*, Comput. Methods. Appl. Mech. Engrg., 198 (2009), pp. 1585–1595, <https://doi.org/10.1016/j.cma.2009.01.012>.
- [36] S. RHEBERGEN AND B. COCKBURN, *A space-time hybridizable discontinuous Galerkin method for incompressible flows on deforming domains*, J. Comput. Phys., 231 (2012), pp. 4185–4204, <https://doi.org/10.1016/j.jcp.2012.02.011>.
- [37] S. RHEBERGEN AND B. COCKBURN, *Space-time hybridizable discontinuous Galerkin method for the advection-diffusion equation on moving and deforming meshes*, in The Courant–Friedrichs–Lewy (CFL) condition, 80 years after its discovery, C. A. de Moura and C. S. Kubrusly, eds., Birkhäuser Science, 2013, pp. 45–63, https://doi.org/10.1007/978-0-8176-8394-8_4.
- [38] S. RHEBERGEN, B. COCKBURN, AND J. J. W. VAN DER VEGT, *A space-time discontinuous Galerkin method for the incompressible Navier–Stokes equations*, J. Comput. Phys., 233 (2013), pp. 339–358, <https://doi.org/10.1016/j.jcp.2012.08.052>.
- [39] B. RIVIÈRE, *Discontinuous Galerkin Methods for Solving Elliptic and Parabolic Equations*, vol. 35 of Frontiers in Applied Mathematics, Society for Industrial and Applied Mathematics, Philadelphia, 2008.
- [40] J. W. RUGE AND K. STÜBEN, *Algebraic multigrid*, in Multigrid methods, SIAM, 1987, pp. 73–130, <https://doi.org/10.1137/1.9781611971057.ch4>.
- [41] D. RUPRECHT, *Wave propagation characteristics of parareal*, Comput. Visual Sci., 19 (2018), pp. 1–17, <https://doi.org/10.1007/s00791-018-0296-z>.

- [42] M. SALA AND R. S. TUMINARO, *A New Petrov–Galerkin Smoothed Aggregation Preconditioner for Nonsymmetric Linear Systems*, SIAM J. Sci. Comput., 31 (2008), pp. 143–166, <https://doi.org/10.1137/060659545>.
- [43] D. SCHÖTZAU AND C. SCHWAB, *Time discretization of parabolic problems by the hp-version of the discontinuous Galerkin finite element method*, SIAM J. Numer. Anal., 38 (2000), pp. 837–875, <https://doi.org/10.1137/S0036142999352394>.
- [44] J. B. SCHRODER, *Smoothed aggregation solvers for anisotropic diffusion*, Numer. Linear Algebra Appl., 19 (2012), pp. 296–312, <https://doi.org/10.1002/nla.1805>.
- [45] W. E. H. SOLLIE, O. BOKHOVE, AND J. J. W. VAN DER VEGT, *Space-time discontinuous Galerkin finite element method for two-fluid flows*, J. Comput. Phys., 230 (2011), pp. 789–817, <https://doi.org/10.1016/j.jcp.2010.10.019>.
- [46] M. TAVELLI AND M. DUMBSER, *A staggered space-time discontinuous Galerkin method for the incompressible Navier–Stokes equations on two-dimensional triangular meshes*, Comput. Fluids, 119 (2015), pp. 235–249, <https://doi.org/10.1016/j.compfluid.2015.07.003>.
- [47] M. TAVELLI AND M. DUMBSER, *A staggered space-time discontinuous Galerkin method for the three-dimensional incompressible Navier–Stokes equations on unstructured tetrahedral meshes*, J. Comput. Phys., 319 (2016), pp. 294–323, <https://doi.org/10.1016/j.jcp.2016.05.009>.
- [48] T. E. TEZDUYAR, M. BEHR, S. MITTAL, AND J. LIOU, *A new strategy for finite element computations involving moving boundaries and interfaces. The deforming-spatial-domain/space-time procedure: II. Computation of free-surface flows, two-liquid flows, and flow with drifting cylinders*, Comput. Methods Appl. Mech. Engrg., 94 (1992b), pp. 353–371, [https://doi.org/10.1016/0045-7825\(92\)90060-W](https://doi.org/10.1016/0045-7825(92)90060-W).
- [49] T. E. TEZDUYAR, S. SATHE, AND K. STEIN, *Solution techniques for the fully discretized equations in computation of fluid-structure interactions with the space-time formulations*, Comput. Methods Appl. Mech. Engrg., 195 (2006), pp. 5743–5753, <https://doi.org/10.1016/j.cma.2005.08.023>.
- [50] J. J. W. VAN DER VEGT AND J. J. SUDIRHAM, *A space-time discontinuous Galerkin method for the time-dependent Oseen equations*, Appl. Numer. Math., 58 (2008), pp. 1892–1917, <https://doi.org/10.1016/j.apnum.2007.11.010>.
- [51] J. J. W. VAN DER VEGT AND H. VAN DER VEN, *Space-time discontinuous Galerkin finite element method with dynamic grid motion for inviscid compressible flows: I. General formulation*, J. Comput. Phys., 182 (2002), pp. 546–585, <https://doi.org/10.1006/jcph.2002.7185>.
- [52] H. VAN DER VEN, *An adaptive multitime multigrid algorithm for time-periodic flow simulations*, J. Comput. Phys., 227 (2008), pp. 5286–5303, <https://doi.org/10.1016/j.jcp.2008.01.039>.
- [53] E. WALHORN, A. KÖLKE, B. HÜBNER, AND D. DINKLER, *Fluid-structure coupling within a monolithic model involving free surface flows*, Comput. Struct., 83 (2005), pp. 2100–2111, <https://doi.org/10.1016/j.compstruc.2005.03.010>.
- [54] L. WANG AND P.-O. PERSSON, *A high-order discontinuous Galerkin method with unstructured space-time meshes for two-dimensional compressible flows on domains with large deformations*, Comput. Fluids, 118 (2015), pp. 53–68, <https://doi.org/10.1016/j.compfluid.2015.05.026>.
- [55] T. WEINZIERL AND T. KÖPPL, *A geometric space-time multigrid algorithms for the heat equation*, Numer. Math. Theory Methods Appl., 5 (2012), pp. 110–130, <https://doi.org/10.1017/S1004897900000258>.

- [56] P. WESSELING AND C. W. OOSTERLEE, *Geometric multigrid with applications to computational fluid dynamics*, J. Comput. Appl. Math., 128 (2001), pp. 311–334, [https://doi.org/10.1016/S0377-0427\(00\)00517-3](https://doi.org/10.1016/S0377-0427(00)00517-3).
- [57] T. A. WIESNER, R. S. TUMINARO, W. A. WALL, AND M. W. GEE, *Multigrid transfers for nonsymmetric systems based on Schur complements and Galerkin projections*, Numer. Linear Algebra Appl., 21 (2014), pp. 415–438, <https://doi.org/10.1002/nla.1889>.
- [58] O. C. ZIENKIEWICZ, R. L. TAYLOR, AND J. Z. ZHU, *The finite element method: its basis and fundamentals*, Elsevier, 2013.
- [59] O. C. ZIENKIEWICZ AND J. Z. ZHU, *A simple error estimator and adaptive procedure for practical engineering analysis*, Int. J. Numer. Methods Eng., 24 (1987), pp. 337–357, <https://doi.org/10.1002/nme.1620240206>.
- [60] O. C. ZIENKIEWICZ AND J. Z. ZHU, *The superconvergent patch recovery and a posteriori error estimates. part 2: Error estimates and adaptivity*, Int. J. Numer. Methods Eng., 33 (1992), pp. 1365–1382, <https://doi.org/10.1002/nme.1620330703>.